Synthesis of Coupled Semiconductor by Filling 1D TiO_2 Nanotubes with CdS

Subarna Banerjee, Susanta K. Mohapatra, Prajna P. Das, and Mano Misra*

Chemical and Materials Engineering, University of Nevada, Reno, Nevada 89557

Received August 22, 2008. Revised Manuscript Received September 15, 2008

A coupled semiconductor material is prepared by filling one-dimensional (1D) titania (TiO_2) nanotubes (NTs) with cadmium sulfide (CdS) nanoparticles (NPs). Self-assembled TiO_2 NTs (length = 550 nm, diameter = 80 nm) are prepared by the sonoelectrochemical anodization method. These NTs are functionalized with CdS NPs by a single-step electrodeposition method. This material harvests solar light in UV as well as visible light (up to 510 nm) region. An eight to 9-fold enhancement in photoactivity is observed using CdS functionalized TiO_2 NTs compared to pure TiO_2 NTs and commercial P25 NPs. This methodology will be useful in designing multijunction semiconductor materials confined inside 1D nanochannels.

1. Introduction

In recent years, there has been a growing interest in finding sustainable alternative energy sources because of the increasing cost of fossil fuels and the drastic effects of global climate change.[1−4] It is envisioned that hydrogen (H_2) has the potential to supplement and ultimately replace fossil fuels. Solar-hydrogen production from water is one of the promising green technologies available today. Generally, this process utilizes a semiconductor material to transfer the solar energy (which is ∼1 kW/(h m^{-2}) on the earth surface) for the production of H_2 from water.[5] Thus, efficient use of sunlight becomes an appealing challenge in developing this technology. Titania (TiO_2) is a widely used semiconductor photocatalyst due to its high stability, favorable band gap energy, abundant availability, and inexpensive cost.[6,7] Because TiO_2 is a large band gap semiconductor (band gap = 3.1−3.2 eV) it absorbs only solar light in the UV region. The major problem is that only about 4−5% of the solar spectrum falls in this UV range. To improve the photocatalytic efficiency, researchers have adopted different strategies such as changing the electrical properties of TiO_2 by varying the crystallite size;[8,9] doping TiO_2 with metal/nonmetal ions in order to induce red shift to the band gap,[10−13] and coupling it with a low band gap semiconductor material, e.g., CdS.[14−19] Among all the TiO_2 nanostructured materials studied in the last three decades, TiO_2 NTs prepared on a Ti foil by the electrochemical anodization method have attracted a lot of attention because of their potential to harvest sunlight and use the photoelectrons efficiently to generate H_2.[20−28] The main advantages of these self-assembled TiO_2 NTs are facile synthesis process, fast charge transport properties and fabrication opportunity, as well as a cost-effective scale-up process (without changing the photoefficiency of the material).[29,30] Recently, it has also been reported that the photoactivity of TiO_2 NTs can be enhanced by sensitizing them with CdS.[19,31,32] Among all the CdS−TiO_2 NTs

* Corresponding author. E-mail: misra@unr.edu.

(1) Turner, J. A. *Science* **1999**, *285*, 687.
(2) Nowotny, J.; Sorrell, C. C.; Sheppard, L. R.; Bak, T *Int. J. Hydrogen Energy* **2005**, *30*, 521.
(3) Kamat, P. V. *J. Phys. Chem. C* **2007**, *111*, 2834.
(4) Blanchette, S., Jr *Energy Policy* **2008**, *36*, 522.
(5) Osterloh, F. E. *Chem. Mater.* **2008**, *20*, 35.
(6) Moon, S.-C.; Mametsuka, H.; Tabata, S.; Suzuki, E. *Catal. Today* **2000**, *58*, 125.
(7) Nowotny, J.; Bak, T.; Nowotny, M. K.; Sheppard, L. R. *Int. J. Hydrogen Energy* **2007**, *32*, 2609.
(8) Ampo, M.; Shima, T.; Kodama, S.; Kubokawa, Y. *J. Phys. Chem.* **1987**, *91*, 4305.
(9) Xu, Y.; Zhu, Z. Z.; Chen, W.; Ma, G. *Chin. J. Appl. Chem.* **1991**, *8*, 28.
(10) Wilke, K.; Breuer, H. D. *J. Photochem. Photobiol., A* **1999**, *121*, 49.
(11) Diebold, U. *Surf. Sci. Rep.* **2003**, *48*, 53.
(12) Thompson, T. L.; Yates, J. T., Jr *Chem. Rev.* **2006**, *106*, 4428.
(13) Park, H.; Vecitis, C. D.; Choi, W.; Weres, O.; Hoffmann, M. R. *J. Phys. Chem. C* **2008**, *112*, 885.
(14) Bessekhouad, Y.; Robert, D.; Weber, J. V. *J. Photochem. Photobiol., A* **2004**, *163*, 569.
(15) Yamada, S.; Nosaka, A. Y.; Nosaka, Y. *J. Electroanal. Chem.* **2005**, *585*, 105.
(16) Kim, J. C.; Choi, J.; Lee, Y. B.; Hong, J. H.; Lee, J. I.; Yang, J. W.; Lee, W. I.; Hur, N. H. *Chem. Commun.* **2006**, 5024.
(17) Jang, J. S.; Li, W.; Oh, S. H.; Lee, J. S. *Chem. Phys. Lett.* **2006**, *425*, 278.
(18) Jang, J. S.; Ji, S. M.; Bae, S. W.; Son, H. C.; Lee, J. S. *J. Photochem. Photobiol., A* **2007**, *188*, 112.
(19) Yin, Y.; Jin, Z.; Hou, F. *Nanotechnology* **2007**, *18*, 495608.
(20) Mor, G. K.; Shankar, K.; Paulose, M.; Vaeghese, O. K.; Grimes, C. A. *Nano Lett.* **2005**, *5*, 191.
(21) Macak, J. M.; Tsuchiya, H.; Ghicov, A.; Schmuki, P. *Electrochem. Commun.* **2005**, *7*, 1133.
(22) Park, J. H.; Kim, S.; Bard, A. J. *Nano Lett.* **2006**, *6*, 24.
(23) Raja, K. S.; Misra, M.; Mahajan, V. K.; Gandhi, T.; Pillai, P.; Mohapatra, S. K. *J. Power Sources* **2006**, *161*, 1450.
(24) Park, J.; Bauer, S.; von der Mark, K.; Schmuki, P. *Nano Lett.* **2007**, *7*, 1686.
(25) Mohapatra, S. K.; Misra, M.; Mahajan, V. K.; Raja, K. S. *J. Phys. Chem. C* **2007**, *111*, 8677.
(26) Mohapatra, S. K.; Misra, M. *J. Phys. Chem. C* **2007**, *111*, 11506.
(27) Albu, S. P.; Ghicov, A.; Macak, J. M.; Hahn, R.; Schmuki, P. *Nano Lett.* **2007**, *7*, 1286.
(28) Chanmee, W.; Watcharenwong, A.; Chenthamarakshan, C.; Kajitvichyanukul, P.; de Tacconi, N. R.; Rajeswar, K. *J. Am. Chem. Soc.* **2008**, *130*, 965.
(29) Mohapatra, S. K.; Mahajan, V. K.; Misra, M. *Nanotechnology* **2007**, *18*, 445705.
(30) Zhu, K.; Neale, N. R.; Miedaner, Frank, A. J. *Nano Lett.* **2007**, *7*, 69.
(31) Sun, W.-T.; Yu, Y.; Pan, H.-Y.; Gao, X.-F.; Chen, Q.; Peng, L.-M. *J. Am. Chem. Soc.* **2008**, *130*, 1124.

10.1021/cm802282t CCC: $40.75
Published on Web 10/22/2008

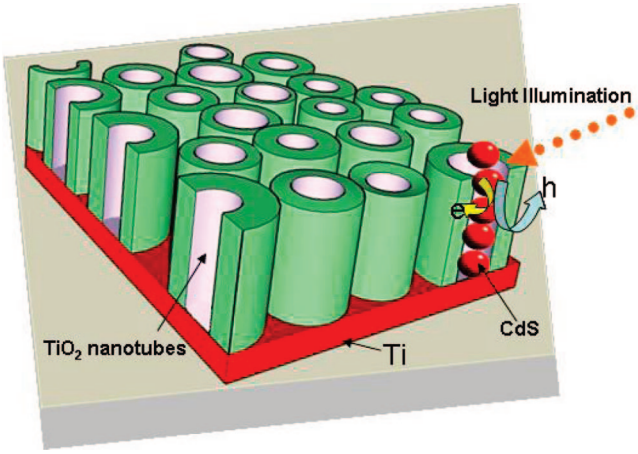

Figure 1. Schematic showing the structure of CdS filled TiO_2 NTs. The photogenerated electrons flow from the conduction band of CdS to the TiO_2 and the holes move toward the surface to generate proton.

integrated electrodes (directly built on Ti metal) designed, the electrode by Sun et al.[31] displayed a lot of promise for hydrogen production from water. However, the reported sequential chemical bath deposition method to synthesize CdS quantum dots into TiO_2 NTs is time-consuming (which is not suitable for practical applications) and produces both hexagonal and cubic (which is not good for photocatalysis) phases of CdS. Here, we report an easy and quick electrochemical process to fill the one-dimensional (1D) TiO_2 NTs with CdS. The electrodeposition method offers an easy control over all these factors, as well as gives a better bonding between the semiconductors.[33,34] This process not only reduces many complicated and time-consuming steps to fabricate the NTs but also gives better stability to the photocatalyst.[9]

The advantages of self-assembled TiO_2 NTs and low band gap compound semiconductors (e.g., CdS) are that they absorb solar-photons efficiently, and also transport the photons to the back contact without much recombination loss. Thus, in a coupled semiconductor in addition to the band edge positions of the two semiconductors, the architecture of the composite material is also very vital. A schematic of the photocatalyst synthesized in this work is depicted in Figure 1. The photoelectrons generated in the CdS NPs pass through the TiO_2 NTs and finally reach the back contact smoothly because of the 1D nature of the NTs. A detailed synthesis process, characterization, and photoactivity of this catalyst will be discussed in this article. The photoresponse of the material under various components of the solar spectrum is also investigated.

2. Materials and Methods

2.1. Materials. Titanium foil (Ti, Alfa-Aesar, 0.127 mm thickness, 99.7% purity on metal basis), phosphoric acid (H_3PO_4, Sigma-Aldrich, 85% in water), sodium fluoride (NaF, Fischer, 99.5%), cadmium chloride ($CdCl_2$, Alfa Aesar, 99%), sodium thiosulfate ($Na_2S_2O_3$, Fischer, 99.8%), sodium sulfide (Na_2S, Sigma-Aldrich, 98%), and sodium sulfite (Na_2SO_3, Sigma-Aldrich, 98%) are used as received.

2.2. Synthesis of TiO_2 NTs. Nanotubular TiO_2 arrays are formed by anodization of the Ti discs in an aqueous solution of 0.5(M) H_3PO_4 and 0.14(M) NaF at pH 2.1. A two-electrode configuration is used for anodization. Ti disk secured in a polytetrafluoroethylene (PTFE) holder exposing an area of 0.7 cm^2 is used as a working electrode. A flag shaped platinum (Pt) electrode (3.75 cm^2) serves as the cathode. Anodization is carried out at room temperature (~24 °C) for 45 min at 20 V_{DC} under ultrasonication. A detailed experimental procedure can be obtained from our previous publication.[35] The anodized samples are properly washed with distilled water to remove the occluded ions, dried in an air oven, and processed for characterization and CdS filling.

2.3. CdS Electrodeposition. CdS is deposited (anodic) from a solution containing 0.2 M $CdCl_2$ and 0.05 M $Na_2S_2O_3$ in 300 mL of deionized (DI) water. The pH is maintained at ~2.1 by adding a few drops of 0.1 M HCl. Initial cyclic voltammetry (CV) experiments have been carried out to find the optimized conditions for a controlled deposition. The experiments are carried out using a computer controlled potentiostat (Schlumberger, model SI-1286, Farnborough, England) and Corrware software (Solartron). The deposition potential and temperature are decided by cyclic voltammetry analysis. A solution temperature of ~70 °C and an applied potential of −0.65 V_{SCE} is found to be the best condition for a fast and controlled deposition.

The CdS deposited TiO_2 (CdS-TiO_2) NTs and pure TiO_2 NTs are annealed in a chemical vapor deposition furnace (CVD, FirstNano) under a nitrogen (N_2) atmosphere at 500 °C for 6 h to convert the amorphous TiO_2 NTs to a crystalline one. The flow rate of N_2 is kept at 200 sccm (standard cubic centimeters per minute) throughout the annealing process. The effect of TiO_2 NTs on the overall photoactivity of the coupled semiconductor is investigated by electrodepositing CdS (for 1000 s at −0.65 V_{SCE}) directly onto Ti foil. The photoactivity of TiO_2 NTs and CdS-TiO_2 NTs are compared with commercial TiO_2 NPs (P25, Degussa). A dip-coating method is adopted to coat the P25 NPs on Ti foil. For this purpose, the P25 NPs (10 mg) are dispersed in a solution containing ethylene glycol (10 mL), ethanol (5 mL), and polyvinylpyrrolidone (5 mg). The Ti foil after P25 coating is dried in an air oven (120 °C) overnight, followed by annealing in an oxygen atmosphere for 3 h at 500 °C. This process removes the organics from the thin layer of P25 and makes a uniform film on the Ti foil.

2.4. Characterization. Both pure TiO_2 NTs and CdS coupled TiO_2 NTs are characterized by various analytical and spectroscopic techniques as discussed below. A scanning electron microscope (SEM; Hitachi, S-4700) is used to analyze the morphology of CdS NPs and TiO_2 NTs. The images are taken in an operating accelerating voltage of 20 kV. Energy dispersive X-ray (EDX) analysis is obtained

(32) Chen, S.; Paulose, M.; Ruan, C.; Mor, G. K.; Varghese, O. K.; Kouzoudis, D.; Grimes, C. A. *J. Photochem. Photobiol., A* **2006**, *177*, 177.
(33) Kadirgan, F.; Mao, D.; Song, W.; Ohno, T.; McCandless, B *Turk. J. Chem.* **2000**, *24*, 21.
(34) Dharmadasa, I. M.; Haigh, J. *J. Electrochem. Soc.* **2006**, *153*, G47.
(35) Mohapatra, S. K.; Misra, M.; Mahajan, V. K.; Raja, K. S. *J. Catal.* **2007**, *246*, 362.

using an Oxford detector. Diffuse reflectance ultraviolet and visible (DRUV−vis) spectra of the samples are measured (to understand the solar light harvesting properties of the materials) from the optical absorption spectra using a UV−vis spectrophotometer (UV-2401 PC, Shimadzu). Fine $BaSO_4$ powder is used as a standard for baseline measurements and the spectra are recorded in a range of 200−800 nm. A scanning transmission electron microscope (STEM; JEOL 2100F) equipped with ESVision software is used for mapping and crystal distribution of the samples. TEM measurements are carried out by scratching a portion of the CdS−TiO_2 sample from the Ti disk in ethanol, followed by ultrasonication for a few minutes for proper distribution. A drop of ethanol (containing sample) is placed on a carbon coated Cu-grid and subjected to high-resolution transmission electron microscopy (HRTEM), STEM and fast Fourier transform (FFT) measurements. Glancing angle X-ray diffraction (GXRD, see the Supporting Information) is done using a Philips 12045 B/3 diffractometer. The target used in the diffractometer is copper ($\lambda = 1.54$ Å), and the scan rate is 1.2°/min.

2.5. Photoelectrochemical (PEC) H_2 Generation. Experiments on H_2 generation from water are carried out in a glass cell with photoanode (pure TiO_2 NTs and CdS-TiO_2 NTs) and cathode (Pt foil) compartments. The compartments are connected by a fine porous glass frit. Ag/AgCl electrode is used as the reference electrode. The cell is provided with a 60 mm diameter quartz window for light incidence. The electrolyte used is an aqueous solution of 0.35(M) Na_2SO_3 and 0.24(M) Na_2S.[36−38] A computer-controlled potentiostat (SI 1286, England) is used to control the potential and record the photocurrent generated. A 300-W solar simulator (69911, Newport-Oriel Instruments, USA) is used as the light source. An AM 1.5 filter is used to obtain one sun intensity, which is illuminated on the photoanode (87 mW/cm^2, thermopile detector from Newport-Oriel is used for the measurements). The samples are anodically polarized at a scan rate of 5 mV/s under illumination and the photocurrent is recorded. All the experiments are carried out under ambient conditions. Electrochemical impedance spectroscopy (EIS) measurements are carried out to understand the charge transport properties of the heterojuncntion electrode. The measurements are done at open circuit potential using similar conditions as described above for PEC tests. The amplitude of the sinusoidal wave is 10 mV and the frequency range examined is 100 kHz to 0.1 Hz.

3. Results and Discussion

3.1. TiO_2 NTs. Self-organized and vertically oriented TiO_2 NT arrays are obtained on a Ti disk (TiO_2/Ti) after an anodization method using H_3PO_4 and NaF. Figure 2 shows the SEM images (surface and cross-sectional views) of self-assembled TiO_2 NT arrays. The average diameter of these NTs is found to be ∼80 nm and the tube length ∼550 nm. The thickness of the wall of the TiO_2 NTs is found to be in the range of 15−20 nm. It is also observed from Figure 2 that the TiO_2 NTs are 1D, compact (NTs are well-attached to each other) and vertically oriented (straight). These as-prepared TiO_2 NTs (on the Ti foil) are used to deposit CdS into the nanochannels of TiO_2 NTs.

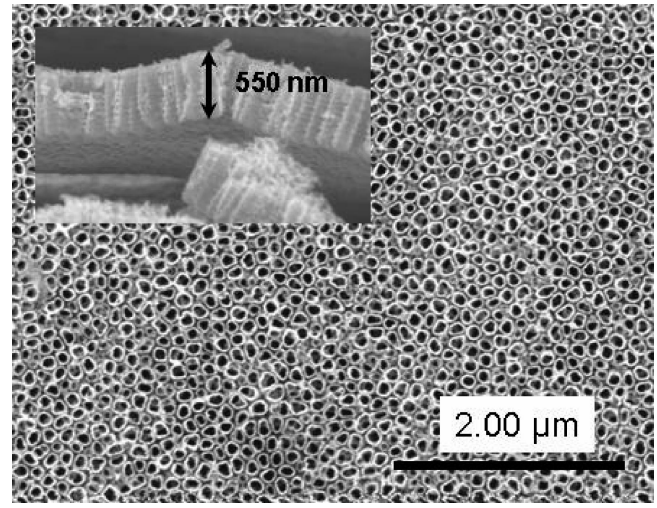

Figure 2. SEM images of as-anodized TiO_2 NTs prepared in an aqueous solution of 0.5 M H_3PO_4 + 0.14 M NaF, pH 2.1. Inset shows the cross-sectional view of the NTs. The internal tube diameter is observed in the range of 80−90 nm and the length of the tubes is observed around 550 nm.

3.2. CdS−TiO_2 NTs. Synthesis of nanostructured CdS with controlled morphology inside alumina, polymers, and mesoporous silica templates is widely known from the literature.[39−42] In this work, we have prepared CdS NPs by confining their architecture inside 1D nanochannels of TiO_2 NT arrays by a simple potentiostatic electrodeposition method. The controlled bottom-up-growth is vital for the synthesis of multijunction materials, which are important because of their unique optical and electronic properties.[43−47] Schmuki and co-workers (*47*) have developed a two step process, the first step involves the reduction of Ti^{4+} to Ti^{3+} at the bottom of the tubes, and then electrodeposition of copper into the TiO_2 NTs. Xie and co-workers have reported the fabrication of nickel oxide (NiO)-embedded TiO_2 NTs for a redox capacitance application.[48] An ultrasonic pretreatment with a nickel salt solution followed by hydrothermal and electrochemical synthesis procedures have been adopted to prepare TiO_2 NTs embedded NiO. In this work, we have successfully deposited CdS inside TiO_2 NTs without

(36) Buhler, N.; Meier, K.; Reber, J.-F. *J. Phys. Chem.* **1984**, *88*, 3261.
(37) Reber, J.-F.; Meier, K. *J. Phys. Chem.* **1984**, *88*, 5903.
(38) Sathish, M.; Viswanathan, B.; Viswanath, R. P. *Int. J. Hydrogen Energy* **2006**, *31*, 891.
(39) Cao, H.; Xu, Y.; Hong, J.; Liu, H.; Yin, G.; Li, B.; Tie, C.; Xu, Z. *Adv. Mater.* **2001**, *13*, 1393.
(40) Zhan, J.; Yang, X.; Wang, D.; Li, S.; Xie, Y.; Xia, Y.; Qian, Y. *Adv. Mater.* **2000**, *12*, 1348.
(41) Wang, S.; Choi, D.; Yang, S. *Adv. Mater.* **2002**, *14*, 1311.
(42) Gao, F.; Lu, Q.; Zhao, D. *Adv. Mater.* **2003**, *15*, 739.
(43) Hao, E.; Sun, H.; Zhou, Z.; Liu, J.; Yang, B.; Shen, J. *Chem. Mater.* **1999**, *11*, 3096.
(44) Bao, H.; Gong, Y.; Li, Z.; Gao, M. *Chem. Mater.* **2004**, *16*, 3853.
(45) Lin, Y.; Tseng, W.; Chang, H.-T. *Adv. Mater.* **2006**, *18*, 1381.
(46) Jiang, W.; Singhal, A.; Zheng, J.; Wang, C.; Chan, W. C. W. *Chem. Mater.* **2006**, *18*, 4845.
(47) Macak, J. M.; Gong, B. G.; Hueppe, M.; Schmuki, P. *Adv. Mater.* **2007**, *19*, 3027.
(48) Xie, Y.; Zhou, L.; Huang, C.; Huang, H.; Lu, J. *Electrochim. Acta* **2008**, *53*, 3643.

any pretreatment of the NTs. The optimization process for a faster deposition and controlled morphology is discussed below.

3.2.1. Optimization of the Electrodeposition Method. CdS is electrodeposited inside TiO_2 NTs using an aqueous solution of $CdCl_2$ and $Na_2S_2O_3$. The reaction mechanism of CdS formation involves electron transfer and subsequent CdS deposition inside the TiO_2 NTs (Equation 1).

$$Cd^{2+} + S_2O_3^{2-} + 2e^- \rightarrow CdS + SO_3^{2-} \qquad (1)$$

The deposition potential and temperature is decided from cyclic voltammetry (figure not presented here). It is observed that CdS deposition is faster around the applied potential of -0.65 V_{SCE}. This potential has been selected for further deposition studies. The deposition current is also observed to increase with the increase in solution temperature and steadies down at around 70 °C. So, a solution temperature of ~70 °C and an applied potential of -0.65 V_{SCE} are found to be the optimum conditions for a fast and controlled anodic deposition.

3.2.2. SEM/EDX. CdS is electrodeposited into the TiO_2 NTs under potentiostatic ($-0.65V_{SCE}$) conditions. A light green colored deposit is observed on the TiO_2 NTs in as little as 100 s. As the deposition time increases, the size of the NPs and surface coverage (on the TiO_2) increases. The color of the surface also changes from light green to yellowish-green (because of quantum size effect). The SEM images of these samples are shown in Figure 3 and the Supporting Information, Figure S1. In the initial phase of deposition, the size of CdS NPs increases linearly with deposition time; however, after 1000 s of deposition, it decreases (Figure 4). This indicates that the deposition rate of CdS slows down after a certain time of deposition. This is due to the fact that CdS is initially deposited on TiO_2 NTs, which follow a faster kinetics. For further deposition, CdS actually gets deposited on the previously deposited CdS layer and not directly onto TiO_2 NTs. CdS is less conducting than TiO_2 and slows down the deposition rate. The sample prepared by 1000 s deposition time is discussed in detail here.

Figure 3 shows the surface and cross-sectional SEM images of a CdS-TiO_2 NTs where deposition time length is 1000 s. It can be seen from the figure that CdS is electrodeposited as spherical NPs on the TiO_2 NTs. A uniform distribution of the NPs with narrow particle size distribution is also noticed from the figure. The cross-sectional view (Figure 3, image B) of the sample depicts CdS NPs as successfully filled inside the TiO_2 NTs. It is also observed that even though the size of the surface CdS NPs increases with deposition time (Figure 4), the growth of the NPs inside the NTs is controlled by the internal diameter of the NTs. This is due to a special constraint inside the NTs. The chemical composition of CdS is determined by EDX spectroscopy and the results are presented in Figure 3 (image A, inset). The EDX spectrum reveals that the NPs deposited on the TiO_2 NTs are mainly composed of cadmium (Cd) and sulfur (S). A Cd/S atomic ratio of ~1 is achieved by this method. The CdS−TiO_2 NTs (1000 s) consists of about 42 wt % CdS. This high loading is due to the filling up of the pore with CdS NPs. The CdS−TiO_2 NTs are

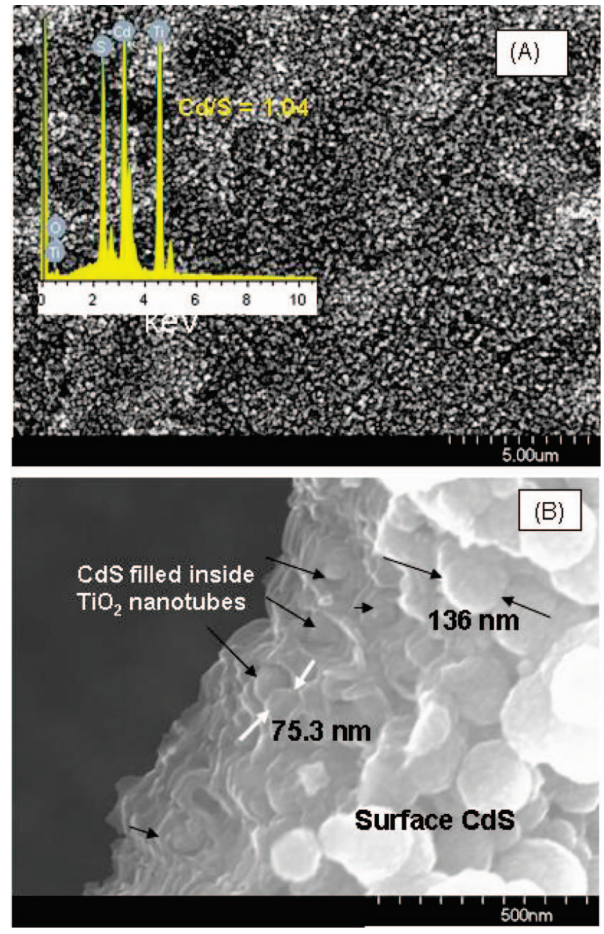

Figure 3. SEM image of as-prepared CdS-TiO_2 NTs: (A) surface view and (B) cross-sectional view. Figure A shows a uniform distribution of CdS NPs on the surface and (B) shows that CdS NPs filled inside the NTs as well. The inset is the EDX spectrum from the surface which shows the Cd/S atomic ratio is ~1.

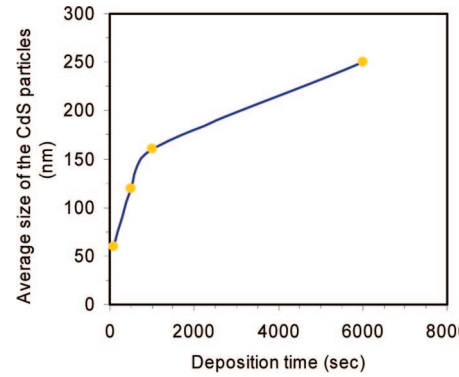

Figure 4. Initially, the diameter of the CdS NPs increased linearly with deposition time, but it does not follow the same profile after a long deposition time.

annealed at 500 °C under a N_2 atmosphere. No change is observed in the morphology and color of the CdS−TiO_2 NTs after annealing. All the as-anodized and annealed samples are found to have good mechanical and thermal stability. The SEM image of CdS deposited on Ti foil (CdS-Ti) reveals a uniform deposition throughout the Ti foil (see the Supporting Information, Figure S2). The CdS particles are also found to have similar size and morphologies compared to the CdS−TiO_2 NTs. The SEM image of P25 coated Ti foil

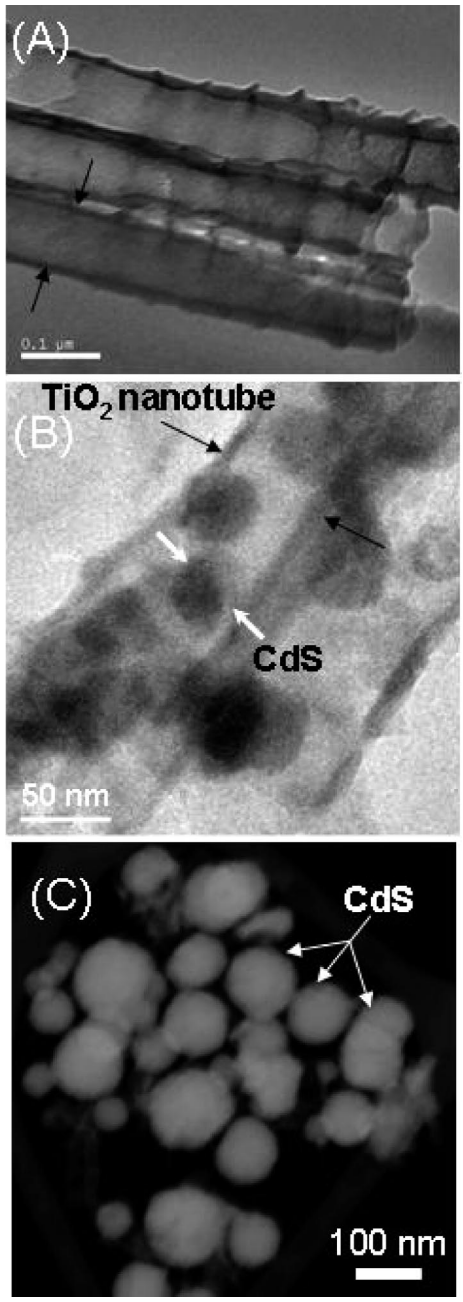

Figure 5. TEM images of (A) TiO_2 NTs, (B) annealed CdS−TiO_2 NTs showing the CdS NPs inside the TiO_2 NTs, and (C) STEM image of CdS NPs (separated from the TiO_2 NTs by ultrasonication).

(P25−Ti) shows a thin and compact film on the Ti foil (see the Supporting Information, Figure S2).

3.2.3. Microstructural Characterization. The annealed CdS−TiO_2 NTs (1000 s) is subjected to TEM and XRD measurements. Figure 5 depicts the TEM images of TiO_2 NTs, CdS NPs inside TiO_2 NTs and isolated CdS NPs deposited on top of TiO_2 NTs (separated from CdS-TiO_2 NTs by ultrasonication for 5 min). The TEM image of TiO_2 NTs shows that the tubes are transparent in nature (Figure 5A). Figure 5B shows the TEM image of TiO_2 NTs filled with CdS NPs (dark spots). The image clearly indicates that the size of the CdS NPs is controlled by the size of TiO_2 NTs. This is supported by our earlier observation in the SEM measurement. A continuous growth of CdS into a nanorod shape is not observed in this process. This might be related

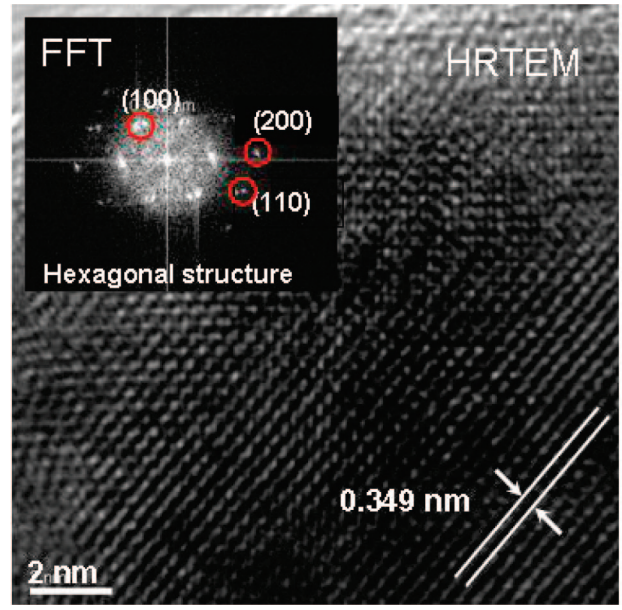

Figure 6. HRTEM image and FFT pattern of a single annealed CdS particle. It shows that CdS nanoparticle is highly crystalline in nature and crystallizes in wurtzite (hexagonal) structure.

to the orientation of the crystal planes in the growth direction. This process can be highly useful in filling the TiO_2 NTs with various semiconductor materials with variable band gap properties to design a one-dimensional multijunction material. A STEM image of the spherical CdS NPs is shown in Figure 5 (image C). The image indicates that the NPs are not agglomerates, but individual and are of uniform size. Figure 6 shows the corresponding HRTEM image of a CdS particle. The lattice fringes of 0.349 nm correspond to the (110) plane of CdS in a wurtzite (hexagonal) crystal system. The inset of Figure 6 presents the fast Fourier-transform (FFT) pattern of the corresponding CdS particle. The FFT pattern reveals a hexagonal arrangement for CdS particles which is in line with the results obtained from HRTEM measurement.[49] The uniform filling of TiO_2 NTs by CdS particles is further confirmed by STEM mapping (see the Supporting Information, Figure S3) through the cross-section of the NTs. The crystalline phases present in the annealed CdS-TiO_2 NTs are obtained from XRD analysis (see the Supporting Information, Figure S4). The XRD pattern shows peaks corresponding to both CdS (wurtzite) and TiO_2 (anatase). It is noteworthy here to mention that the process adopted by Sun et al.[31] produced a mixture of hexagonal and cubic phases of CdS; however, in this work a single phase (hexagonal) CdS is obtained. A single-phase nanocrystalline material is very useful in photovoltaic and PEC research because of its high charge-transport properties and low recombination losses. From the above results and discussion, we infer that the material prepared here is highly crystalline in nature, which is essential for a good photocatalytic material.

To check the suitability of the CdS−TiO_2 NTs for PEC applications, absorption studies are carried out. Figure 7 depicts the DRUV−vis spectra of CdS-TiO_2 NTs (sample prepared in 1000 s deposition) and pure TiO_2 NTs. It has

(49) Warner, J. H.; Tilley, R. D. *Adv. Mater.* **2005**, *17*, 2997.

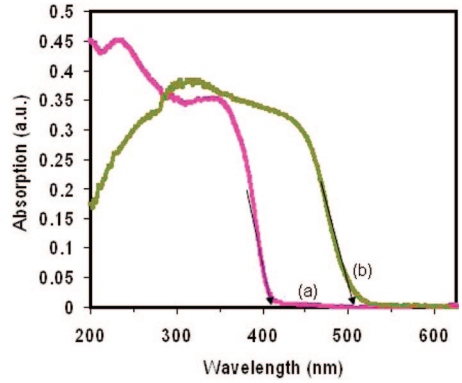

Figure 7. DRUV−vis spectra of annealed (a) TiO_2 NTs and (b) CdS−TiO_2 NTs (1000 s deposited sample). CdS−TiO_2 NTs absorbs light up to 510 nm (E_g = 2.43 eV), whereas TiO_2 absorbs only up to 410 nm (E_g = 3.02 eV).

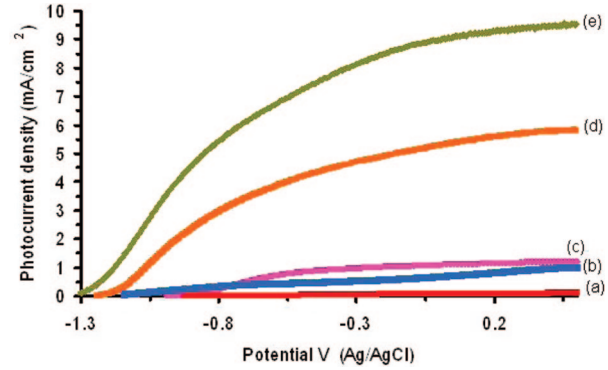

Figure 8. (a) Photocurrent obtained from CdS−TiO_2 NTs under dark (no illumination) conditions, (b) P25−Ti under illumination (c) TiO_2 NTs under illumination (d) CdS−Ti under illumination and (e) CdS−TiO_2 NTs under illumination conditions. A simulated solar light (AM 1.5 conditions, 87 mW/cm^2) is used for illumination. The measurements are carried out in sulfide−sulfite electrolyte. All the samples are annealed before used.

been observed that TiO_2 absorbs in the UV region with a band edge ~410 nm (band gap, E_g = 3.02 eV). On the other hand, the spectrum of CdS−TiO_2 NTs absorbs both in UV as well as visible region with a band edge of 510 nm (E_g = 2.43 eV). These studies show that the CdS−TiO_2 NTs thus prepared (by combining the absorption properties of TiO_2 NTs in the UV region and CdS NPs in the visible region) absorbs in the visible as well as in the UV region of the solar spectrum. By increasing the deposition time (i.e., increasing the size of the CdS NPs), the λ_{max} is shifted (408 nm at 100 s to 473 nm in 6000 s deposition time sample) toward more the visible light region (red shift), which is due to the quantum size effect (see the Supporting Information, Figure S5). In the high loading sample (6000 s sample) the absorption of the sample in the UV region (which corresponds to TiO_2 NTs) decreases because of a thick layer of CdS being deposited on the TiO_2 NTs. The sample prepared in 1000 s is used to evaluate the photoactivity of the material.

3.3. PEC Activity. It is known that the photoactivity for H_2 production increases considerably in coupled semiconductors because of the interparticle electron transfer process.[50] In a coupled semiconductor, the photogenerated electron is transferred from one semiconductor to the other easily. This is due to the favorable position of the conduction bands in the semiconductor couple which results in efficient electron transfer for H^+ ion reduction. In this article, CdS−TiO_2 NTs is tested for solar H_2 generation from water.

The CdS−TiO_2 NTs (exposed area = 0.7 cm^2) thus prepared is used as photoanode in the PEC cell to evaluate its photoactivity to generate H_2 from water in sulfide-sulfite (S^{2-}/SO_3^{2-}) electrolyte under simulated solar light illumination (87 mW/cm^2). The PEC tests are carried out using Pt as cathode and Ag/AgCl as a reference electrode. The PEC activities of CdS-TiO_2 NTs under dark and illumination conditions are presented in Figure 8. The results depict the generation of H_2 through PEC reaction in terms of the photocurrent obtained from the PEC cell using various photoanodes. The obtained photocurrent is compared with the amount of H_2 evolved from the cathode compartment. This is carried out by downward displacement of water. The amount of H_2 evolved is found equivalent to the amount of current generated in the cell (i.e., it follows Faraday's law). This confirms that the obtained current in the cell is due to the H_2 evolution and not the photoetching of the catalyst. All the results presented here are in the form of photocurrent density.

The CdS−TiO_2 NTs do not show significant activity without light illumination (i.e., under dark condition). On the other hand, under illumination conditions, a maximum photocurrent density of 9.5 mA/cm^2 is obtained at 0.5 $V_{Ag/AgCl}$ from the photoanode. For a comparison, the photoactivity of pure TiO_2 NTs, TiO_2 NPs (P-25 on Ti metal) and CdS NPs (on Ti metal) under illumination condition are also included in the figure. The photoactivity of CdS−TiO_2 NTs is observed to be 8−9-fold more compared to the TiO_2 NTs (1.21 mA/cm^2) and TiO_2 NPs (1.07 mA/cm^2) photoanode. The CdS−Ti electrode also shows good activity (5.82 mA/cm^2) compared to the TiO_2 electrodes (both NTs and NPs); however, its activity is ~40% less than the composite electrode (CdS−TiO_2 NTs). These results confirm that the TiO_2 NTs, as well as the CdS NPs contribute significantly to the overall H_2 generation of the composite material.

The effect of CdS concentration on the photoactivity of CdS-TiO_2 NTs is also investigated and the results are depicted in the Supporting Information, Figure S6. The figure shows that the photocurrent density increases with an increase in CdS loading up to 42 wt % (1000 s deposited sample). However, when the CdS loading is increased to 65 wt % (at 6000 s deposition) the photoactivity of the CdS−TiO_2 NTs decreases (see the Supporting Information, Figure S6). This might be due to a very high CdS loading, which reduces the activity contributed by the TiO_2 NTs and the CdS NPs inside the NTs, ultimately decreasing the overall photoactivity of the material. This observation is supported by UV−vis absorption studies of various CdS loaded TiO_2 NTs (see the Supporting Information, Figure S5), which shows a decrease in UV absorption of the material after a 6000 s deposition. Further information about the contribution of the UV and visible components of the solar spectrum is obtained using a band-pass filter (Edmund Optics, $\lambda \geq 420$ nm). It is interesting to note that 68% of the photoactivity of CdS−TiO_2 NTs is contributed by the visible components,

(50) Serpone, N.; Lawless, D.; Khairutdinov, R. *J. Phys. Chem.* **1995**, *99*, 16646.

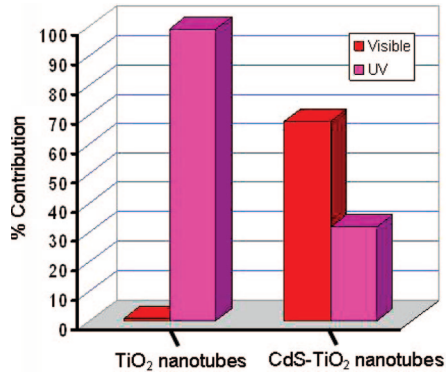

Figure 9. Contribution of visible and ultraviolet components of the solar spectrum to the overall activity of the TiO_2 NTs and annealed CdS-TiO_2 NTs. TiO_2 NTs only showed 0.8% (out of 1.21 mA/cm^2) and CdS−TiO_2 NTs showed 68% (out of 9.5 mA/cm^2). The UV and visible light contribution is calculated by doing one experiment under AM 1.5 conditions and one more using a cut off filter (visible light illumination, $\lambda \geq 420$ nm).

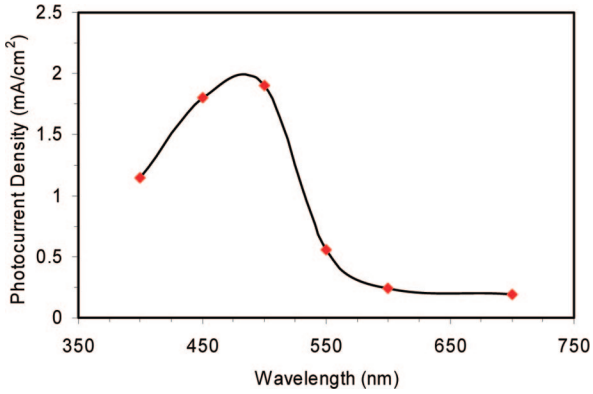

Figure 10. Contribution of various wavelength regions to the photoactivity of N_2 annealed CdS−TiO_2 NTs. The current density (calculated from the potentiodynamic plots at 0.2 $V_{Ag/AgCl}$) versus wavelength of light illuminated. Interference filters (Edmund optics) with CWL of ± 15 nm and fwhm of 50 nm are used for the potentiodynamic measurements. It shows that most of the activities are contributed from the solar spectrum of wavelength in the range of ≤550 nm.

whereas pure TiO_2 NTs showing a majority of their activity in the UV region contributes to the rest of the photoactivity (Figure 9). Further, spectral response of the cell, i.e., the wavelength dependence of the photocurrent is measured using various filters in conjugation with the AM 1.5 filter. Filters with 50 nm intervals are used in the range of 400 to 650 nm Edmund Optics, CWL ± 15 nm and fwhm = 50 nm). It is observed that photons in the range of 400−550 nm only contribute to the photoactivity of the composite material (Figure 10). There is no significant contribution from the spectrum having $\lambda \geq 550$. This can be explained from the DRUV−vis studies presented in Figure 7. The absorption profile of the CdS−TiO_2 NTs shows no significant absorption in the wavelengths greater than 550 nm. The above results suggest that the photoactivity of the current catalyst can be improved further by coupling this with another semiconductor (e.g., CdSe or Fe_2O_3)[51,52] which absorbs photons having $\lambda \geq 550$.

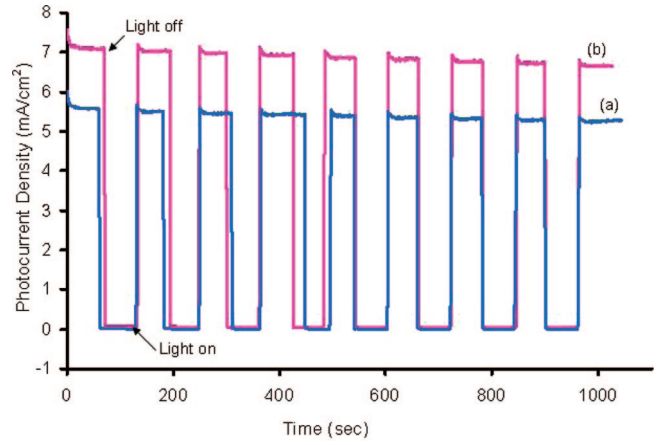

Figure 11. Potentiostatic hydrogen generation from annealed CdS−TiO_2 NTs photoanode at (a) −0.4$V_{Ag/AgCl}$ and (b) −0.6$V_{Ag/AgCl}$. The photocurrent became almost zero when the light is switched off (illumination stopped) and the original photocurrent again came back after illumination.

The information on the charge transport properties of the TiO_2 NTs and the CdS−TiO_2 coupled semiconductor electrode is obtained from EIS analysis. Figure S7 in the Supporting Information shows a typical EIS plot for a TiO_2 NTs and CdS−TiO_2 NTs electrode under illumination conditions in sulfide-sulfite electrolyte. The *x* axis and *y* axis represent the real part of the impedance (Z') and the imaginary part of the impedance (Z''), respectively. The measured EIS spectra are observed as depressed semicircles and the origin of the deviation is from the presence of inhomogeneities and porosity in the electrode, which gives rise to a frequency dependent penetration depth for the ac wave.[53] It is found that only one capacitance arc is observed on the EIS Nynquist plot. The arc sizes are almost identical for both TiO_2 NTs and CdS−TiO_2 NTs electrodes. This indicates that the charge transfer resistance remains unchanged after the deposition of CdS. The slight decrease in resistance is due to the decrease in resistance on the solid−liquid interface after the CdS deposition. This indicates that the electrodeposition technique employed here gives rise to a good interaction of the CdS NPs with the NTs (better Ohmic contacts), and as a result gives rise to an efficient and faster charge transfer through the coupled semiconductor.

The photoresponse of the CdS−TiO_2 NTs is carried out by potentiostatic (current vs time, $I-t$) measurements under intermittent illumination. Figure 11 shows the $I-t$ curve obtained from the PEC cell containing CdS−TiO_2 NTs as photoanode and Pt as cathode at two different potentials (−0.4 $V_{Ag/AgCl}$ and −0.6 $V_{Ag/AgCl}$). The photocurrent value goes down to zero as soon as the illumination of light on the photoanode is stopped, and the photocurrent comes back to the original value as soon as light is illuminated again on the sample. It indicates that the current observed for this cell is completely due to the photoactivity of the catalyst and that the charge-transport properties are very fast.

3.4. Working Principle of CdS−TiO_2 Coupled Semiconductor System. The overall photoconversion efficiency of a multiband gap semiconductor depends on the

(51) Kongkanand, A.; Tvrdy, K.; Takechi, K.; Kuno, M.; Kamat, P. V. *J. Am. Chem. Soc.* **2008**, *130*, 4007.
(52) Kay, A.; Cesar, I.; Grätzel, M. *J. Am. Chem. Soc.* **2006**, *128*, 15714.
(53) Macdonald, D. D.; McKubre, M. C. H. *ASTM Spec. Tech. Publ.* **1981**, *110*, 198.

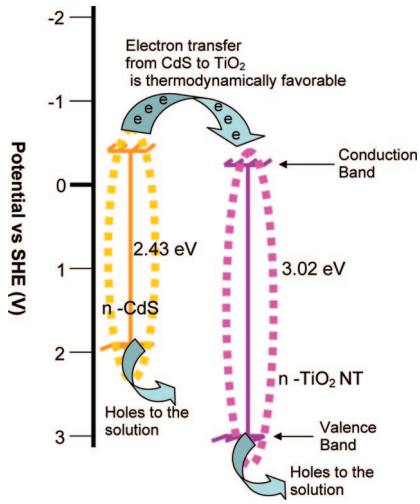

Figure 12. Schematic showing the thermodynamically favorable conduction bands for CdS and TiO_2. The photoelectrons generated in CdS conduction band-pass to the conduction band of TiO_2 NTs and then get transferred to the solution (through back contact) for the reduction of proton to generate hydrogen. The holes (from both CdS and TiO_2) move to the interface to react with the electrolyte to generate protons.

position of its conduction and valence bands as well as their geometrical arrangement. For efficient interparticle electron transfer between the semiconductors CdS and TiO_2, the conduction band of TiO_2 must be more anodic than the corresponding band of the sensitizer, i.e., CdS. These thermodynamic conditions also favor the phenomenon of electron injections, and thus CdS and TiO_2 match very well (Figure 12).[50] When the system is under UV−vis irradiation, both semiconductors (CdS and TiO_2) are excited; electrons are injected from CdS to TiO_2 as in the case of visible illumination. In addition to this, more photoelectrons are generated from TiO_2 NTs by harvesting UV photons. In this case, a high concentration of electrons is obtained in the conduction band of TiO_2 compared to TiO_2 alone. In addition to the thermodynamically favorable energy bands, geometrical architecture of the composite is also an important factor which controls the lifetime of charge carriers. The 1D TiO_2 NTs collect the photoelectrons from CdS and pass through them to the back contact. The holes (from both CdS and TiO_2) generated in the process are transferred to the solid−liquid interface to generate protons from the solution. In this process, each mole of water gives rise to one mole of H_2 (please see the Supporting Information for details).[54−56]

There are no significant changes observed in the surface morphology (by SEM, see Figure S8 in the Supporting Information) and absorption profile (by DRUV−vis, see Figure S9 in the Supporting Information) of the composite photoanode after the sample has been used for PEC tests for 10 h. These results show that the composite photocatalyst has potential for long-term operation with good photoactivity. The postmeasurement characterization of the catalyst and H_2 measurements from the cathode compartment clearly shows that this cell behaves as a normal PEC system. Further investigation is going on to identify the possible minor photocorrosion problem.

4. Conclusions

In conclusion, we report the synthesis of a photocatalyst by filling TiO_2 nanotubular arrays with CdS NPs by a simple electrodeposition method. This architecture leads to better solar light harvesting in the visible light region. An 8−9-fold enhancement in photoactivity is observed between the CdS functionalized TiO_2 NTs and pure TiO_2 NTs. The visible light components ($\lambda \geq 420$ nm) contribute around 68% of the total photocurrent generated from the CdS−TiO_2 NTs. Better absorption and Ohmic contact between the two semiconductors leads to better photoactivity. This approach to design photocatalyst by filling 1D NTs will give a new direction in the field of multijunction solar-cell material.

Acknowledgment. This work has been sponsored by the U.S. Department of Energy through DOE Grant DE-FC36-06GO86066. The authors thank Dr. Mo Ahmedian, University of Nevada Reno, Reno, NV, for the TEM and STEM measurements.

Supporting Information Available: Figures S1−S9 and mechanism of H_2 evolution (PDF). This material is available free of charge via the Internet at http://pubs.acs.org.

CM802282T

(54) Meissner, D.; Benndorf, C.; Memming, R. *Appl. Surf. Sci.* **1987**, *27*, 423.
(55) Ashokkumar, M *Int. J. Hydrogen Energy* **1998**, *23*, 427. references are cited therein.
(56) Linkous, C. A.; Muradov, N. Z.; Ramser, S. N *Int. J. Hydrogen Energy* **1995**, *20*, 701.